Supporting Information

For

Developing deep blue (CIE_y < 0.08) and pure blue (CIE_y < 0.11) OLEDs via molecular engineering of carbazole moiety

Wenkui Wei,[a] Jiuyan Li,[a]* Di Liu,[a,b]* Yongqiang Mei,[a] Ying Lan,[a] Houru Tian,[a] Rui Niu,[a] Botao Liu[a]

[a] State Key Laboratory of Fine Chemicals, College of Chemical Engineering, Dalian University of Technology, 2 Linggong Road, Dalian, 116024, China.

E-mail: jiuyanli@dlut.edu.cn, liudi@dlut.edu.cn

[b] State Key Laboratory of Luminescent Materials and Devices, South China University of Technology, Guangzhou, 510640, China.

Contents

1. Instruments and methods

General information

The ^{1}H NMR and ^{13}C NMR spectra were recorded using a 400 MHz and 126 MHz Bruker AVANCE II 400 and Bruker AVANCE III 500. The mass spectra were recorded on a matrix-assisted laser desorption/ionization (MALDI) and time of flight (TOF) micro mass spectrometry (MS) and HP1100LC/MSD MS spectrometer. Elemental analyses were carried out on a Carlo-Eriba 1106 elemental analyzer. The UV-vis absorption spectra measurements were performed on a Perkin-Elmer Lambda 650 spectrophotometer. The LTFL and LTPH spectra were measured in 2-MeTHF glass matrix at 77 K using a Hitachi F-4600 fluorescence spectrometer. All PL spectra and temperature dependent transient PL decay spectra were measured with an Edinburgh FLS1000 fluorescence spectrophotometer. Thermogravimetric analysis (TGA) was performed on a Perkin-Elmer thermogravimeter (Model TGA7) under a nitrogen gas flow at a heating rate of 10 °C min^{-1}. Cyclic voltammetry (CV) measurements were carried out by using a conventional three-electrode configuration and an electrochemical workstation (CHI610E) at a scan rate of 100 mV s^{-1}. A glass carbon working electrode, a platinum-wire counter electrode, and a saturated calomel electrode (SCE) reference electrode were used. All of the measurements were performed at room temperature on samples dissolved in DCM (positive mode) and in DMF (negative mode), deoxygenated with nitrogen gas, and with 0.1 M Bu_4NPF_6 as the supporting electrolyte. The optimized molecular structures at ground state were calculated using the density functional theory (DFT) and time-dependent density

functional theory (TD-DFT) method. All the calculations were performed using the Gaussian 09 program package.

Device fabrication

The pre-cleaned indium tin oxide (ITO) glass substrates, with a sheet resistance of 15 Ω m^{-2}, were treated by UV-ozone for 30 min. A 40 nm thick PEDOT: PSS film was spin-coated on the ITO glass substrate firstly and baked at 120 ℃ for 30 min in air. Subsequently, the substrate was transferred into a vacuum chamber to deposit the organic layers with a base pressure of less than 10^{-6} Torr (1 Torr =133.32 Pa). A 1 nm thin layer of LiF and a subsequently 200 nm thin layer of Al were vacuum deposited as the cathode. Deposition rates are 0.1 Å s^{-1} for LiF and 6 Å s^{-1} for Al. The emitting area of each pixel was determined by the overlapping of the two electrodes and was 9 mm^2. The EL spectra, CIE coordinates and *J-V-B* characteristics of the devices were measured with a PR705 photometer and a source-measure-unit Keithley 236 under ambient conditions at room temperature. The forward viewing external quantum efficiency was calculated by using the current efficiency, EL spectra and human photopic sensitivity.

Materials

Unless otherwise described, all reagents and anhydrous solvents were purchased from commercial sources and used as received. The hole transporting materials (TAPC), host materials (DPEPO) and electron transporting materials (TmPyPB and TPBi) were purchased from Lumtec Co., Ltd. The exciton blocking material (mCP)

was purchased from Xi'an Polymer Light Technology Corp.

Calculation formulas for the photophysical parameters

In light of the TADF character of TMCz-DMTD, we calculated its photophysical parameters of the doped film by implementing the following equations [1]:

$k_F = \Phi_F/\tau_F$

$\Phi_{PL} = k_F/(k_F + k_{IC})$

$\Phi_F = k_F/(k_F + k_{IC} + k_{ISC})$

$\Phi_{ISC} = k_{ISC}/(k_F + k_{IC} + k_{ISC})$

$k_{TADF} = \Phi_{TADF}/(\Phi_{ISC}\ \tau_{TADF})$

$k_{RISC} = k_F\ k_{TADF}\ \Phi_{TADF}/(k_{ISC}\ \Phi_F)$

$\Phi_{TADF}/\Phi_F = (\Phi_{ISC}\ \Phi_{RISC})/(1 - \Phi_{ISC}\ \Phi_{RISC})$

where Φ_{PL} is the total fluorescence quantum yield; Φ_F is the prompt fluorescence decay component of Φ_{PL}; Φ_{TADF} is the delayed fluorescence decay component of Φ_{PL}; τ_F is the lifetime of prompt fluorescence; τ_{TADF} is the lifetime of TADF; k_F is the rate constant of fluorescence; k_{IC} is the rate constant of internal conversion; k_{TADF}, k_{ISC}, k_{RISC} are the rate constants of TADF, intersystem crossing and reverse intersystem crossing, respectively; Φ_{ISC} and Φ_{RISC} are the quantum efficiencies of ISC and RISC processes, respectively.

2. Synthesis and characterizations

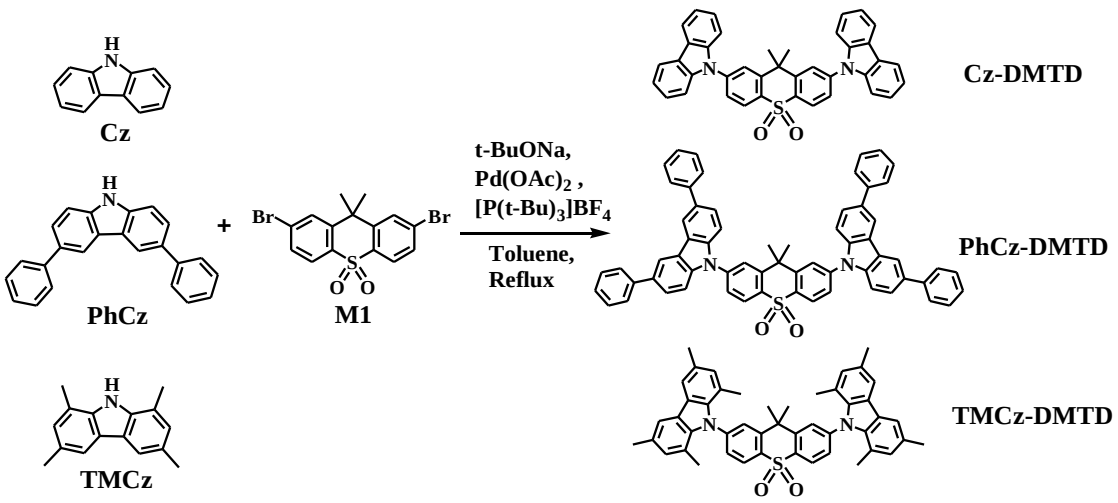

Scheme S1. Synthetic routes of Cz-DMTD, PhCz-DMTD and TMCz-DMTD.

Cz was purchased from commercial sources and used as received. PhCz, TMCz and intermediate M1 were synthesized according to the literature methods [2-4].

General procedure for the synthesis of Cz-DMTD, PhCz-DMTD and TMCz-DMTD: M1 (450 mg, 1.08 mmol), Cz or PhCz or TMCz (2.38 mmol) and sodium tert-butoxide (208 mg, 2.16 mmol) were dissolved into 30 ml toluene in a 100 ml round-bottom three-neck flask. Under nitrogen atmosphere, palladium acetate (12.14 mg, 0.05 mmol) and tri-tert-butylphosphonium tetrafluoroborate (47.06 mg, 0.16 mmol) were added into the system. After further degassing for 15 min, the reaction mixture was heated to 110 ℃, stirring overnight. After the system was cooled to room temperature, the solvent was removed in reduced pressure. The residues were extracted with dichloromethane, washed with water and dried over $MgSO_4$. Further purification through column chromatography with petroleum ether/dichloromethane as eluents gave the pure final products as white powders.

Cz-DMTD: Yield: 80%. ^{1}H NMR (400 MHz, Chloroform-*d*), δ (ppm): 8.53 (d, *J* = 8.3 Hz, 2H), 8.20 (d, *J* = 7.7 Hz, 4H), 8.06 (s, 2H), 7.85 (d, *J* = 8.3 Hz, 2H), 7.50 (s, 4H), 7.50 (s, 4H), 7.38 (m, 4H), 2.04(s, 6H). ^{13}C NMR (126 MHz, Chloroform-*d*), δ (ppm): 147.81, 142.18, 140.14, 134.98, 126.46, 125.79, 124.18, 123.94, 120.92, 120.64, 109.45, 39.96, 31.00. MALDI-TOF-MS (*m*/*z*): cal. for $C_{39}H_{28}N_2O_2S$ 588.1866 $[M]^+$; found 588.1901. Anal. Calcad for $C_{39}H_{28}N_2O_2S$: C, 79.57; H, 4.79; N, 4.76; S, 5.45; Found: C, 79.54; H, 4.75; N, 4.78; S, 5.50.

PhCz-DMTD: Yield: 72%. ^{1}H NMR (400 MHz, Chloroform-*d*), δ (ppm): 8.58 (d, *J* = 8.3 Hz, 2H), 8.46 (s, 4H), 8.13 (s, 2H), 7.91 (d, *J* = 8.3 Hz, 2H), 7.78 (s, 4H), 7.77 (s, 8H), 7.59 (d, *J* = 8.5 Hz, 4H), 7.55 (m, 8H), 7.41 (m, 4H), 2.10 (s, 6H). ^{13}C NMR (126 MHz, Chloroform-*d*), δ (ppm): 147.93, 142.14, 141.48, 140.03, 135.11, 134.70 128.89, 127.32, 126.91, 126.62, 126.17, 125.67, 124.66, 124.04, 119.17, 109.89, 40.07, 31.09. MALDI-TOF-MS (*m*/*z*): cal. for $C_{63}H_{44}N_2O_2S$ 892.3118 $[M]^+$; found 892.3154. Anal. Calcad for $C_{63}H_{44}N_2O_2S$: C, 84.72; H, 4.97; N, 3.14; S, 3.59; Found: C, 84.76; H, 5.02; N, 3.11; S, 3.56.

TMCz-DMTD: Yield: 71%. ^{1}H NMR (400 MHz, Chloroform-*d*), δ (ppm): 8.37 (d, *J* = 8.17 Hz, 2H), 7.87 (s, 2H), 7.79 (s, 4H), 7.73 (d, *J* = 8.12 Hz, 2H), 6.97 (s, 4H), 2.51 (s, 12H), 1.89 (s, 12H), 1.85 (s, 6H). ^{13}C NMR (126 MHz, Chloroform-*d*), δ (ppm): 147.14, 145.87, 139.21, 136.56, 130.58, 129.76, 129.04, 124.54, 120.81, 118.06, 39.37, 30.85, 21.08, 19.80. MALDI-TOF-MS (*m*/*z*): cal. for $C_{47}H_{44}N_2O_2S$ 700.3118 $[M]^+$; found 700.3099. Anal. Calcad for $C_{47}H_{44}N_2O_2S$: C, 80.54; H, 6.33; N, 4.00; S, 4.57; Found: C, 80.58; H, 6.34; N, 3.97; S, 4.56.

3. Supplementary tables and figures

Table S1. Photophysical parameters of PhCz-DMTD and TMCz-DMTD in the doped films (7 wt% in DPEPO).

emitters	Φ_F (%)	Φ_{TADF} (%)	τ_F (ns)	τ_{TADF} (μs)	k_F (10^7 s^{-1})	k_{IC} (10^7 s^{-1})	k_{ISC} (10^7 s^{-1})	k_{TADF} (10^5 s^{-1})	k_{RISC} (10^5 s^{-1})	Φ_{ISC} (%)	Φ_{RISC} (%)
PhCz-DMTD	56.7	-	3.8	-	14.6	4.11	-	-	-	-	-
TMCz-DMTD	50.4	7.3	10.0	2.6	5.04	3.69	1.27	2.22	1.28	12.7	100.0

Table S2. Summary of device performances for the reported TMCz based OLEDs.

Emitters	Host	B_{max} (cd m^{-2})	EQE_{max} (%)	λ_{EL} (nm)	CIE (x, y)	FWHM (nm)	Ref.
TMCz-DMTD	**DPEPO**	**647**	**8.7**	**447**	**(0.157, 0.107)**	**65**	**This work**
4	PPF	~11000	13.3	~467	(0.14, 0.16)	~68	5
Cz-TRZ2	DPEPO	~11000	22.0	~487	-	~85	2
MCz-XT	PPF	~500	11.1	485	(0.18, 0.44)	~83	6
tMCzPN	DPEPO	~1100	26.0	500	(0.20, 0.42)	90	7
tmCzAZB	mCP	~6000	12.4	464	(0.14, 0.15)	62	8
MCz-BOBO	PPF	5700	20.1	473	(0.13, 0.20)	61	9
MCz-BSBS	PPF	13600	25.9	484	(0.14, 0.33)	64	9
TMCz-BO	PPF	5900	20.7	471	(0.14, 0.18)	59	10
TMCz-3P	PPF	6500	20.4	479	(0.14, 0.26)	61	10
MCz-TXT	mCBP	22100	25.8	497	(0.21, 0.46)	~85	11
MCz-XT	mCBP	17700	25.5	489	(0.19, 0.42)	~79	11

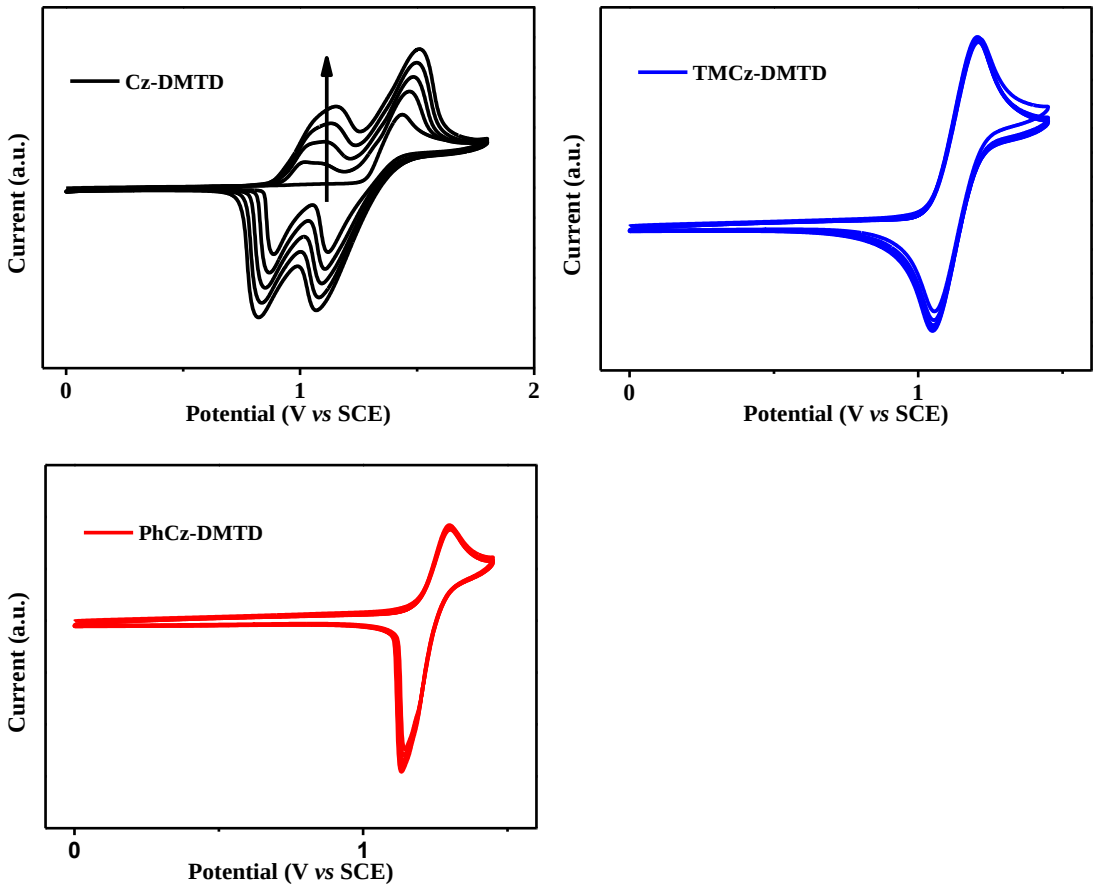

Fig. S1 Repeated cyclic voltammograms (oxidation) for Cz-DMTD, PhCz-DMTD and TMCz-DMTD in DCM.

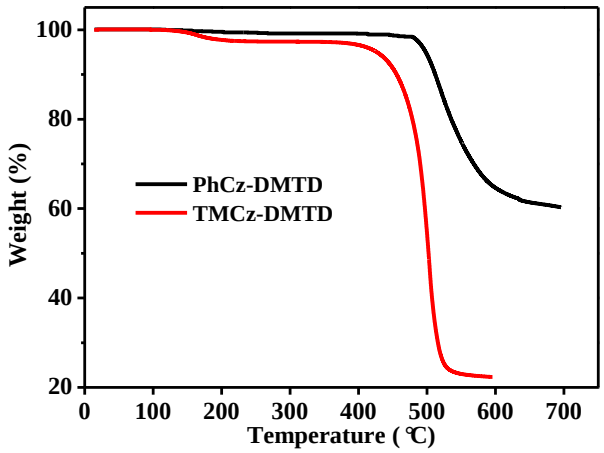

Fig. S2 TGA thermograms of PhCz-DMTD and TMCz-DMTD recorded at a heating rate of 10 ℃ min^{-1}.

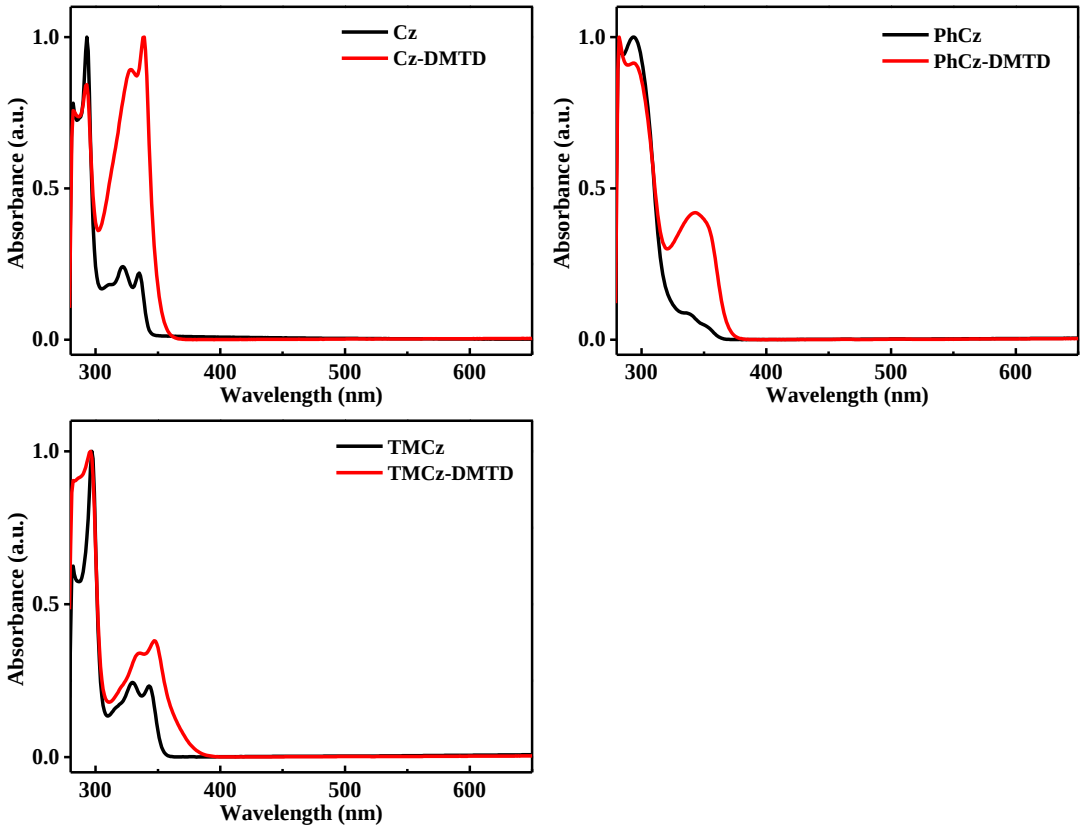

Fig. S3 UV-vis absorption spectra of Cz-DMTD, PhCz-DMTD, TMCz-DMTD and their corresponding donors in toluene.

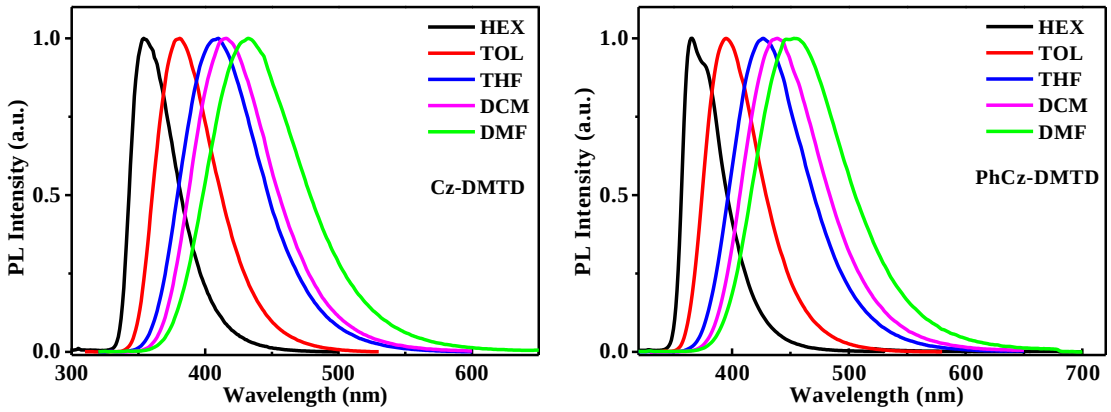

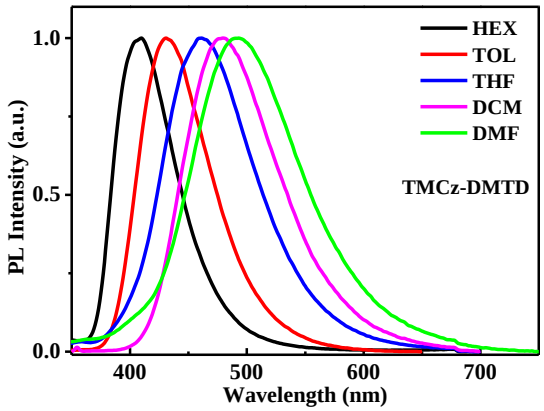

Fig. S4 PL spectra of Cz-DMTD, PhCz-DMTD and TMCz-DMTD in HEX, TOL, tetrahydrofuran (THF), DCM, and DMF at room temperature.

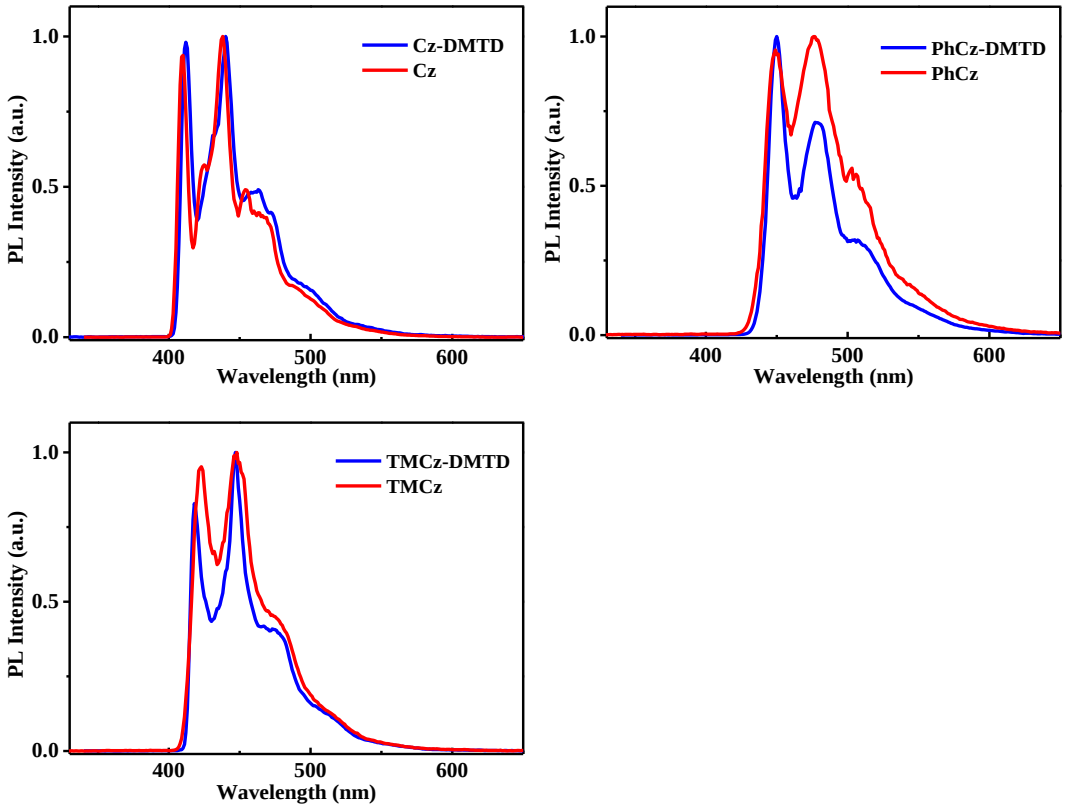

Fig. S5 LTPH spectra of Cz-DMTD, PhCz-DMTD, TMCz-DMTD and their corresponding donors in frozen 2-MeTHF at 77 K.

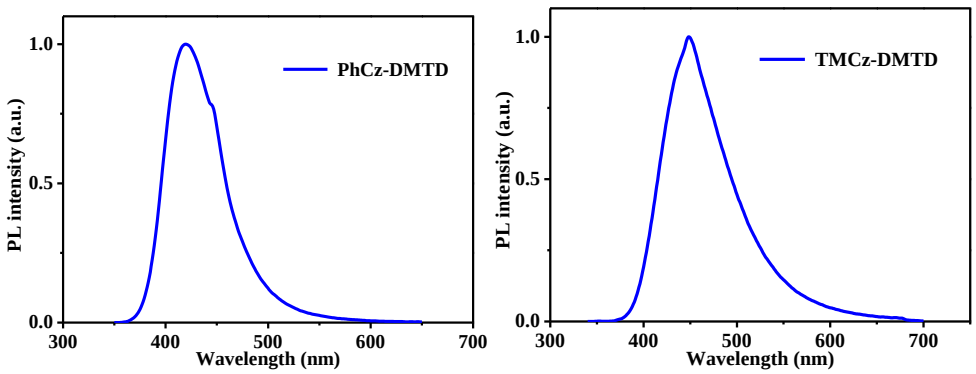

Fig. S6 PL spectra of doped films at room temperature under N_2.

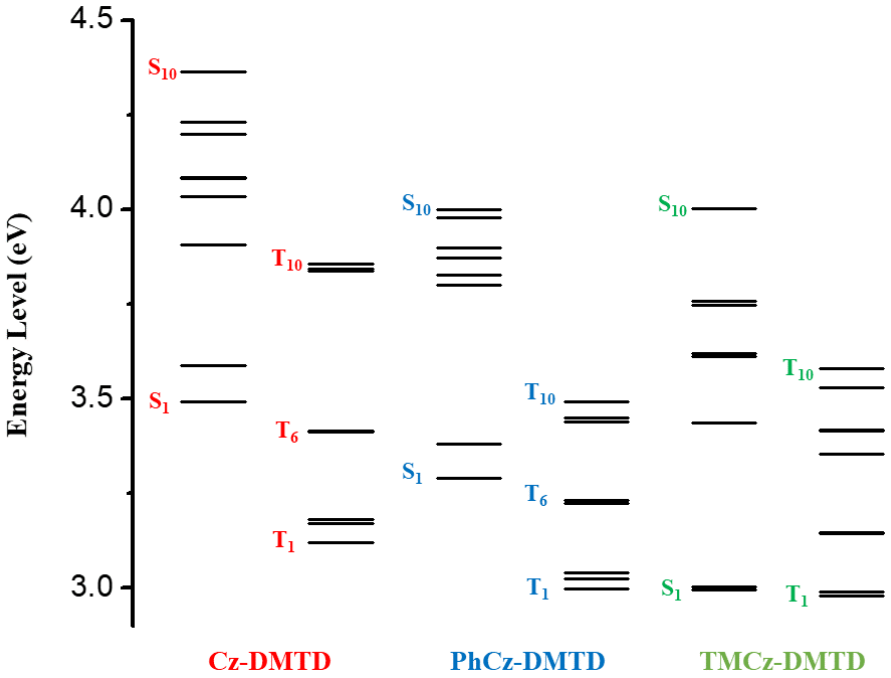

Fig. S7 Energy levels of first-tenth singlet/triplet excited states of Cz-DMTD, PhCz-DMTD, TMCz-DMTD from TD-DFT calculations.

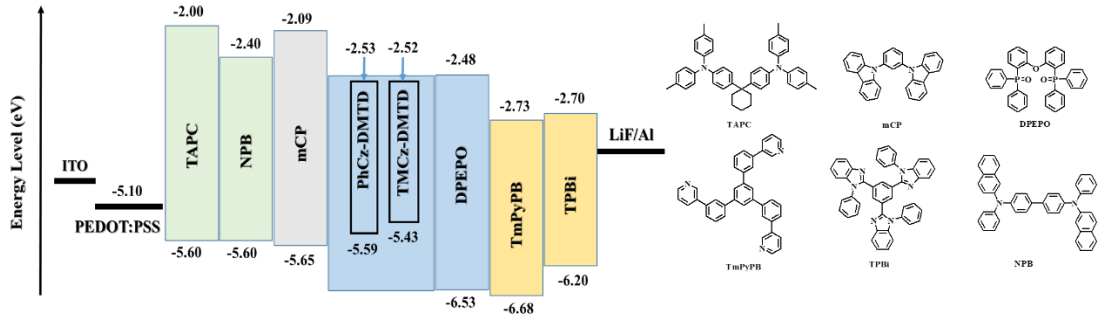

Fig. S8 Energy level diagrams of the OLEDs based on PhCz-DMTD, TMCz-DMTD and the molecular structures of organic functional materials.

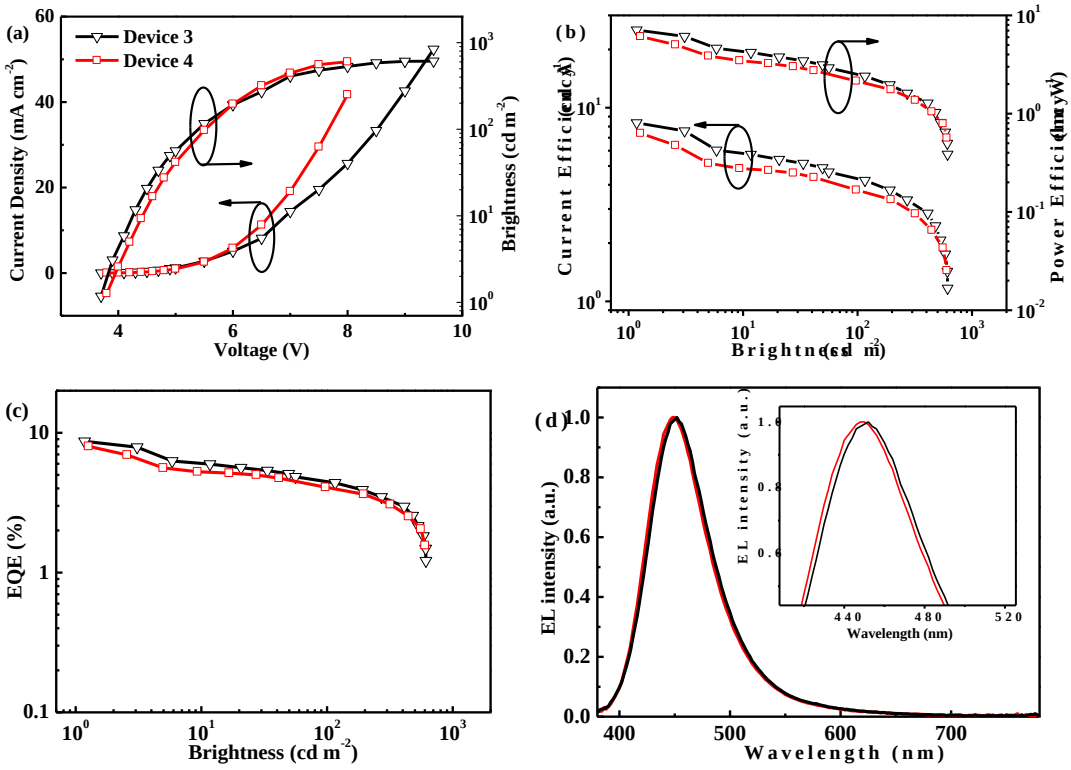

Fig. S9 *J-V-B* characteristics (a), CE-*B*-PE characteristics (b), EQE-*B* curves (c) and EL spectra (d),of device 3 and device 4.

Reference

1 T. Yang, Z. Cheng, Z. Li, J. Liang, Y. Xu, C. Li and Y. Wang, *Adv. Funct. Mater.*, 2020, **30**, 2002681.

2 L.-S. Cui, H. Nomura, Y. Geng, J. U. Kim, H. Nakanotani and C. Adachi, *Angew. Chem., Int. Ed*, 2017, **56**, 1571-1575.

3 C. Fu, S. Luo, Z. Li, X. Ai, Z. Pang, C. Li, K. Chen, L. Zhou, F. Li, Y. Huang and Z. Lu, *Chem. Commun.*, 2019, **55**, 6317-6320.

4 Y.-L. Zhang, Q. Ran, Q. Wang, Q.-S. Tian, F.-C. Kong, J. Fan and L.-S. Liao, *Org. Electron.*, 2020, **81**, 105660.

5 M. Numata, T. Yasuda and C. Adachi, *Chem. Commun.*, 2015, **51**, 9443-9446.

6 J. Lee, N. Aizawa, M. Numata, C. Adachi and T. Yasuda, *Adv. Mater.*, 2017, **29**, 1604856.

7 J.-L. Cai, W. Liu, K. Wang, J.-X. Chen, Y.-Z. Shi, M. Zhang, C.-J. Zheng, S.-L. Tao and X.-H. Zhang, *Front. Chem.*, 2019, **7**, doi: 10.3389/fchem.2019.00017

8 T. L. Wu, S. H. Lo, Y. C. Chang, M. J. Huang and C. H. Cheng, *ACS Appl. Mater. Interfaces*, 2019, **11**, 10768-10776.

9 T. Agou, K. Matsuo, R. Kawano, I. S. Park, T. Hosoya, H. Fukumoto, T. Kubota, Y. Mizuhata, N. Tokitoh and T. Yasuda, *ACS Mater. Lett.*, 2020, **2**, 28-34.

10 J. U. Kim, I. S. Park, C.-Y. Chan, M. Tanaka, Y. Tsuchiya, H. Nakanotani and C. Adachi, *Nat. Commun.*, 2020, **11**, 1765.

11 N. Aizawa, A. Matsumoto and T. Yasud, *Sci. Adv.*, 2021, **7**, eabe5769.